NANO LETTERS

pubs.acs.org/NanoLett

Letter

Disentangling Structural and Electronic Properties in V_2O_3 Thin Films: A Genuine Nonsymmetry Breaking Mott Transition

Federico Mazzola,*[,⊥] Sandeep Kumar Chaluvadi,[⊥] Vincent Polewczyk, Debashis Mondal, Jun Fujii, Piu Rajak, Mahabul Islam, Regina Ciancio, Luisa Barba, Michele Fabrizio, Giorgio Rossi, Pasquale Orgiani, and Ivana Vobornik

Cite This: *Nano Lett.* 2022, 22, 5990−5996

Read Online

ACCESS | Metrics & More | Article Recommendations | Supporting Information

ABSTRACT: Phase transitions are key in determining and controlling the quantum properties of correlated materials. Here, by using the combination of material synthesis and photoelectron spectroscopy, we demonstrate a genuine Mott transition undressed of any symmetry breaking side effects in the thin films of V_2O_3. In particular and in contrast with the bulk V_2O_3, we unveil the purely electronic dynamics approaching the metal−insulator transition, disentangled from the structural transformation that is prevented by the residual substrate-induced strain. On approaching the transition, the spectral signal evolves slowly over a wide temperature range, the Fermi wave-vector does not change, and the critical temperature is lower than the one reported for the bulk. Our findings are fundamental in demonstrating the universal benchmarks of a genuine nonsymmetry breaking Mott transition, extendable to a large array of correlated quantum systems, and hold promise of exploiting the metal−insulator transition by implementing V_2O_3 thin films in devices.

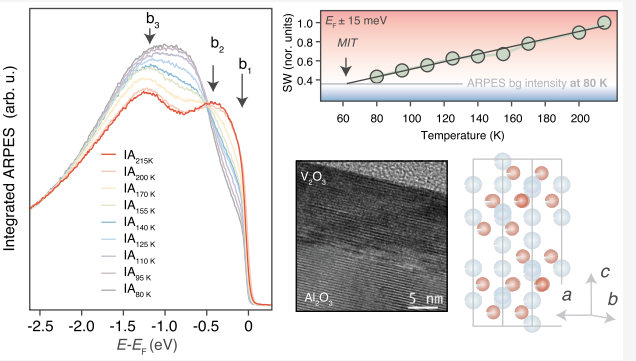

KEYWORDS: *Metal−insulator transition, V_2O_3, Mott transition, ARPES*

The ability of manipulating electronic states in quantum matter is a milestone for the condensed matter physics community. Materials with properties lying at the verge of an instability have attracted attention because even small external stimuli could drive them into completely different electronic and/or magnetic configurations. V_2O_3 is a typical example: upon lowering the temperature (in bulk form[1]), it exhibits a metal−insulator transition (MIT) accompanied by antiferromagnetism and a rhombohedral−monoclinic structural transformation.[2−6] The attention garnered by this material is not fortuitous. Such a MIT spans over 10 orders of magnitude in resistivity in a hysteretic fashion, which is fundamental for applications[7−13] in electronics such as oscillators, neuromorphic devices, and memory; yet the impossibility of tuning such a transition due to the structural breakdown has hindered its exploitation in oxide electronics. Moreover, it was for long considered to be the only physical realization of a genuine Mott transition, e.g., exemplified by the single-band Hubbard model.[14,15] However, its structural complexity, the multiorbital nature and the concurrent metal−insulator, paramagnetic−antiferromagnetic, and rhombohedral−monoclinic transitions, have challenged that simple picture. Indeed, a combined LDA + DMFT calculation by Poteryaev et al.[16] unveiled a mechanism for the paramagnetic MIT in V_2O_3, which was mostly driven by the orbital degrees of freedom. Specifically, electronic correlations were shown to substantially enhance the low-energy effective trigonal crystal-field splitting between the lower e_g^{π} doublet and the upper a_g^1 singlet. Such an enhancement leads to a nearly empty a_g^1 electron pocket at the Fermi level and a highly incoherent nearly half-filled e_g^{π} band amenable to Mott's localization and magnetism. This mechanism, which seems to explain observed photoinduced insulator-to-metal transitions,[9,17] has been later questioned by angle-resolved photoemission spectroscopy (ARPES) data in metallic V_2O_3 at 200 K, i.e., above the T_{MIT} of 165 K.[18] Here, a Fermi surface composed by both a_g^1 and e_g^{π} was found, not compatible with a system at the verge of an a_g^1−e_g^{π} gap opening and selective e_g^{π} Mott's localization. Therefore, despite considerable efforts, the mechanism leading to the MIT of V_2O_3 and its claimed entanglement with the rhombohedral-to-monoclinic structural transitions remains an

Received: June 7, 2022
Revised: June 29, 2022
Published: July 5, 2022

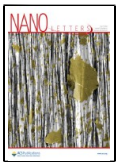

https://doi.org/10.1021/acs.nanolett.2c02288
Nano Lett. 2022, 22, 5990−5996

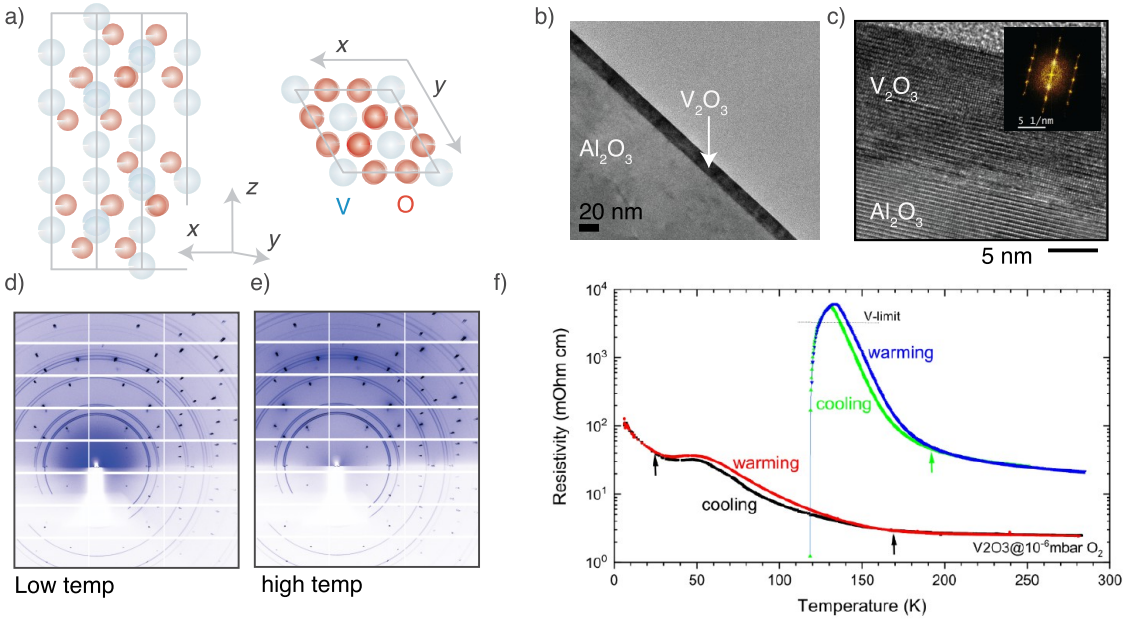

Figure 1. (a) Crystal structure of V_2O_3 along with the real space unit cell vectors. Both side and top view are reported. (b, c) Low- and high-magnification HRTEM micrographs of V_2O_3 on Al_2O_3 (in the inset the Fourier transform of the image), respectively. (d, e) Grazing-incidence XRD maps at high temperature (i.e., room temperature) and low temperature (i.e., about 96 K on the sample) of a representative 15 nm V_2O_3 film on Al_2O_3 (diffraction rings are related to residual silver paste used to ground the sample and on the back of substrate). (f) Resistivity measurements for samples grown with a mildly different oxygen pressure, namely, 7×10^{-7} mbar (green/blue curves) and 1×10^{-6} mbar (black-red lines), respectively. The green arrow indicates the beginning of the hysteresis for the green-blue resistivity curve. Similarly, the black arrows indicate the beginning and the end of the hysteresis in the extra-oxygenated sample (black-red lines).

unsolved mystery after more than a century of extensive investigation.

Here, by using strain-engineering thin film technology, we froze the crystal structure of thin V_2O_3 films and thus succeeded in studying the pure electronic behavior of the system undergoing the MIT disentangling it from the structural transition. After performing precise thin-film growth via in situ pulsed laser deposition (PLD), we exploited ARPES with polarized synchrotron light to identify the dominant orbital character of the measured electronic bands. Finally, we disclosed the full temperature evolution of the spectroscopic features approaching the MIT, providing a strong experimental evidence for a genuine Mott transition, void of symmetry breaking. Transport measurements and temperature dependent X-ray diffraction (XRD) confirm a hysteretic behavior in the resistivity with the lack of any structural changes within the same temperature interval. This indicates that the onset of the hysteresis has a purely electronic nature, in agreement with previous thin-films transport measurements[19] but opposite from that conjectured for the bulk.[20] In our ARPES data, the transition critical point is preceded by a continuous and gradual disappearance of spectral weight at the Fermi level, accompanied by a lack of k_F variation, consistent with avoided structural transition. This trend on approaching the critical temperature is consistent with the Mott transition described by DMFT[21] and in contrast to the abrupt first order character observed for bulk V_2O_3.

V_2O_3 films were grown on (0001)-oriented Al_2O_3 by PLD.[22] The sample temperature was kept at ∼700 °C and in an oxygen background pressure of 7×10^{-7} mbar throughout the growth. After deposition, films were cooled down to room temperature under the same deposition pressure. The typical deposition rate was about 3.5 Å ·min^{-1}, thus allowing a full control of the film thickness. All of the investigated samples were 15 nm thick. In situ X-ray absorption spectroscopy (XAS) did not show any line-shape difference in the V $L_{2,3}$ edges from the reference bulk material and the V_2O_3 films at room temperature.[23]

Structural properties of V_2O_3 films were investigated by ex situ XRD. While thick films (e.g., 80 nm)[23,24] behave like bulk samples,[25] in thinnest (i.e., <15 nm) films, the out-of-plane lattice parameter shifted to lower values (i.e., 13.92 Å with respect to the bulk value of 14.0161 Å).[25] This effect confirms that the samples under investigation are in nature different from the bulk. Nevertheless, identifying the precise strain mechanism induced by the substrate is not a trivial task. As a matter of fact, by considering the film/substrate lattice parameters (Al_2O_3 unit cell a = 4.7605 Å and c = 12.9956 Å; V_2O_3 unit cell, a = 4.9424 Å and c = 14.0161 Å), a possible substrate-driven compressive strain would correspond to an increase of V_2O_3 c-lattice parameter, which (on the contrary) was found to reduce.[26] Despite of this, the restoring of the bulk-like properties of V_2O_3 in very thick films clearly indicates the crucial role of the substrate in determining the structural properties of the very thin films. The atomic structure of the V_2O_3 films was investigated by high-resolution transmission electron microscopy (HRTEM). The structure of the film over the whole image is homogeneous, with a very smooth surface and free of significant defects. No structural differences were detected among the near-interface region and far from it, as well as no traces of spurious phases or segregation of crystalline phases other than V_2O_3, while structural dislocations are mostly present at the film/substrate interface. The fast Fourier transformation (FFT) patterns can be safely assigned to the corundum-phase structure.[25] In order to investigate the occurrence of corundum-to-monoclinic phase transition in

https://doi.org/10.1021/acs.nanolett.2c02288
Nano Lett. 2022, 22, 5990−5996

thin films, variable-temperature grazing-incidence XRD (GIXRD) measurements (panels d and e in Figure 1) were performed at the X-ray diffraction beamline 5.2 at Elettra (Trieste, Italy). GIXRD measurements (see also Supporting Information) confirmed the absence of any structural change from high temperature (i.e., 300 K) down to our minimum temperature allowed by the setup (96 K on the sample). As a matter of fact, the diffraction pattern remains exactly the same, while major differences would have been observed for a monoclinic structural phase at low T.[1] This is the crucial difference between our thin films and the bulk sister compounds, where a strong crystal symmetry breaking occurs at 165 K.[1] Transport properties were probed by a four-points DC technique and reported in Figure 1 f. The thickest samples (i.e., 80 nm) grown at 7×10^{-7} mbar do show bulk-like behavior characterized by the opening of the hysteresis at about 195 K (blue-green curves) but with its closing above the V-limit of the current source and therefore not detectable. Following a previous report,[27] thin films were also grown by slightly increasing the background O_2 pressure (i.e., 1×10^{-6} mbar) to lower enough their resistivity values and thus being able to observe both the closing of the hysteresis and the truly insulating regime characterized by the opening of a gap in the V_2O_3 band structure. It is worth underlining that, as reported in literature,[28] overoxygenated samples (i.e., $V_2O_{3.02}$) keep on being structurally arranged in the corundum phase with a slight lowering of the T_{MIT}, thus suggesting the insertion of extra oxygens in the interstitial atomic sites.

The ARPES measurements were performed in ultrahigh vacuum ($<1 \times 10^{-10}$ mbar) at the APE-LE beamline at Elettra, with a Scienta DA30 hemispherical electron energy analyzer and with linearly polarized photons of 72 eV. The samples were transported under UHV conditions (1×10^{-10} mbar) from the PLD to the ARPES chamber; thus the samples' surface was not exposed to ambient conditions or to external contaminants. In our setup, the light impinges on the (001) surface with a 45° incidence angle so that the plane identified by the light wave-vector $\mathbf{q}$ and the c-axis of the sample corresponds to a mirror plane of the $R\bar{3}c$ space group of the corundum structure, which we conventionally take as the $y-z$ plane (panel a in Figure 2). The light polarization is either parallel to the axis perpendicular to that mirror plane, in our convention parallel to the x-axis (polarization $E_s = (1,0,0)$), or perpendicular to it and to $\mathbf{q}$ (polarization $E_p = (0,1,1)/\sqrt{2}$).

In our adopted geometry (Figure 2a), the Γ−K high symmetry direction of the paramagnetic metallic phase of V_2O_3 is along x axis. In this configuration we find that the photoemission matrix elements are favorable and the spectral intensity is prominent. The O_{2p} states and the V_{3d} bands are easily identified in the spectra. The former disperse at high binding energies, with their maximum at 4 eV below the Fermi energy while the V_{3d} bands extend closer to E_F with a bandwidth of about 2 eV. In the metallic paramagnetic phase, at least three sets of bands are recognizable within the energy range between −1.5 eV and the Fermi level (Figure 2b,c). We refer to each manifold with b_i (i = 1, 2, 3) and start discussing their main features at high temperature (i.e., $T = 230$ K). In order to better identify the orbital character of the signal, we analyze the polarization dependence at the high symmetry Γ point, and from them we can extract the purely in-plane (E_s) and out-of-plane ($E_d = 2E_s - E_p$) polarization contributions that derive from the e_g^{π} and a_g^1 orbitals, respectively.

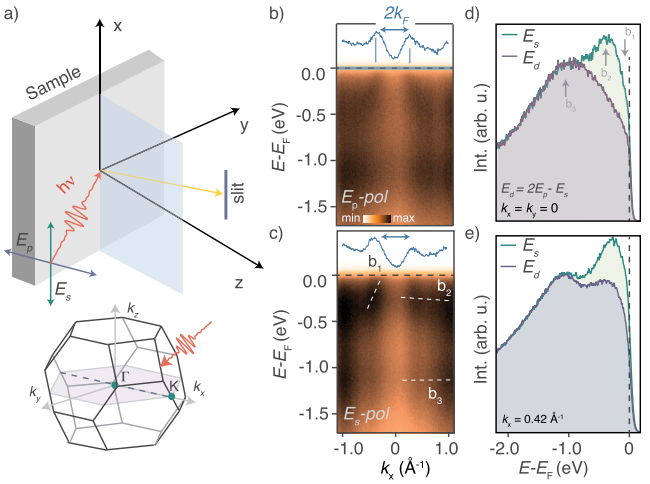

Figure 2. (a) Experimental geometry with the relevant scattering plane and light polarization vector and the three-dimensional Brillouin zone. Γ−K direction is by the green dots. (b, c) ARPES measurements at 230 K for E_s and E_p polarizations ($h\nu$ = 72 eV) showing sensitivity to the orbital character. Three bands are visible and indicated with b_1, b_2, and b_3. (d) Γ point ($k_x = k_y = 0$) E_s and E_d ($2E_p - E_s$) polarizations energy distribution curves showing a strong dichroism for b_2 which indicates a prominent e_g^{π} character and a mixed orbital signal (e_g^{π} and a_g^1) for b_3. (e) Dichroism spectra for energy distribution curves at $k_x \geq k_F$ ($k_y = 0$, $k_x = 0.42$ Å^{-1}), highlighting the orbital character for b_1 away from the Γ point. The evident difference in the signals allows us to demonstrate the e_g^{π} character for this band. The same result can be found for any other value of $k_x \geq k_F$.

The nearly dispersionless feature b_3 lies around −1.2 eV below the Fermi level and has a rather broad photoemission signal which is basically the same for E_s and E_d light polarizations (see Figure 2d for the spectra at $k_x = k_y = 0$, i.e., at the Γ point). We associate b_3 with the lower Hubbard band with all t_{2g} orbitals equally populated, thus an e_g^{π}:a_g^1 occupation ratio of 2:1 compatible with previous results in the low temperature antiferromagnetic insulating phase.[29] The manifold b_2 lies around −0.3 eV below the Fermi level and shows a very weak but still evident dispersion. The dependence of its photoemission signal upon light polarization suggests that b_2 has dominant e_g^{π} character (Figure 2d). We do not find evidence that b_2 crosses the Fermi level upon increasing k_z from Γ toward the Z point, which would thus lead to the electron pocket observed by Lo Vecchio et al.,[18] at the (100) surface. We believe that this might be due to the presence of a dead layer[30,31] more pronounced at the (001) surface than at the (100) one (as conjectured in ref 18). As a matter of fact, the dead layer mechanism is more effective for the out-of-plane orbital components, i.e., the a_g^1, and therefore, it is expected to play a major role at the (001) surface compared to the (100). This is compatible with our evidence that b_2 has mostly e_g^{π} character rather than the a_g^1 one. Finally, the metallic band b_1 disperses crossing the Fermi level with a nearly circular hole-like Fermi surface of radius 0.36 ± 0.02 Å^{-1}, corresponding to an electron filling fraction of 0.76 ± 0.6. Although the maximum of b_1 is not visible in our data, the polarization dependence of the signal above k_F still suggests a prevailing e_g^{π} character (Figure 2e). Overall, our high temperature data are in agreement with those reported for the same sample orientation in the literature.[18]

https://doi.org/10.1021/acs.nanolett.2c02288
Nano Lett. 2022, 22, 5990−5996

At lower temperatures, significant differences in the measured thin film V_2O_3electronic structure arise. ARPES measurements at 80 K (Figure 3a) mainly show a loss of

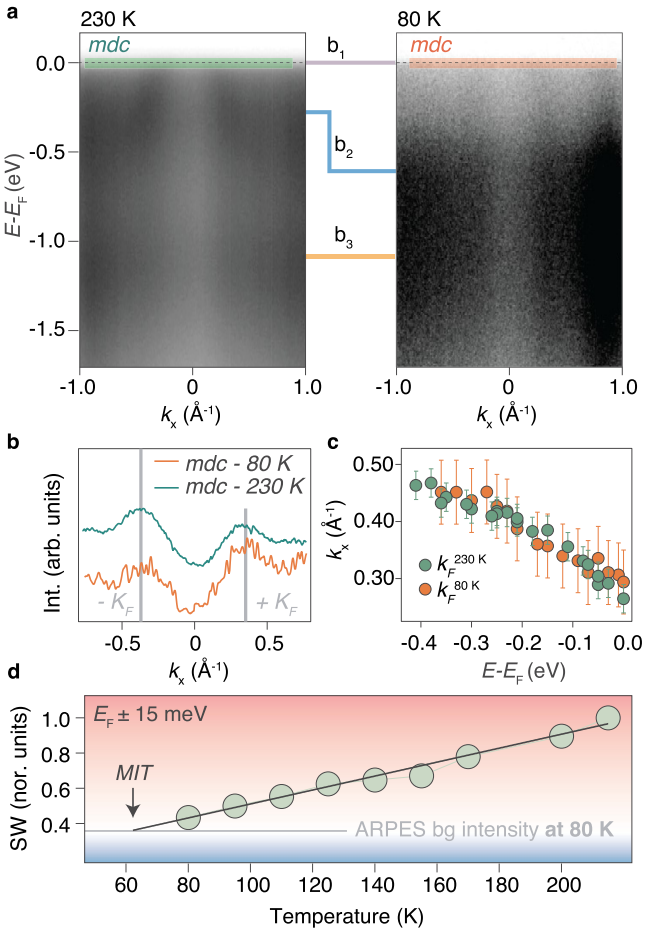

Figure 3. (a) ARPES measurements (at 72 eV) at 230 K (left) and 80 K (right). (b) Fermi level wave-vectors reported for both temperatures showing in both cases the same value. This indicates that negligible change in the band b_1 is detected at the Fermi level. (c) Fitted positions of the band b_1 (average of left and right branches reported) showing that the band remains the same throughout the temperature range. (d) Trend of the ARPES spectral weight at the Fermi level showing a perfectly linear decrease in the intensity of b_1. From this trend, we extrapolate that b_1 will vanish at the extrapolated temperature of 62 K.

spectral weight for the b_1 band and a shift in energy of about 340 meV of the b_2 band. Despite the spectral weight loss, we find that b_1 always crosses the Fermi level at a wave-vector that remains stable from 230 K down to 80 K (see Figure 3b). The spectral weight of b_1 diminishes linearly as a function of temperature, allowing us to extrapolate a tentative metal−insulator transition critical temperature as the one at which the b_1 spectral weight at E_F becomes comparable to the background intensity. Such temperature, as indicated in Figure 3d, is around $T_{MIT} = 62$ K, which is significantly lower than the bulk value of 165 K. The decrease of the b_1 intensity is compensated by a similar increase in the signal of b_3, as shown in Figure 4 (panel c). However, the b_2 signal remains constant at all temperatures. The observed transfer of spectral weight is reminiscent of an electronically driven Mott transition.

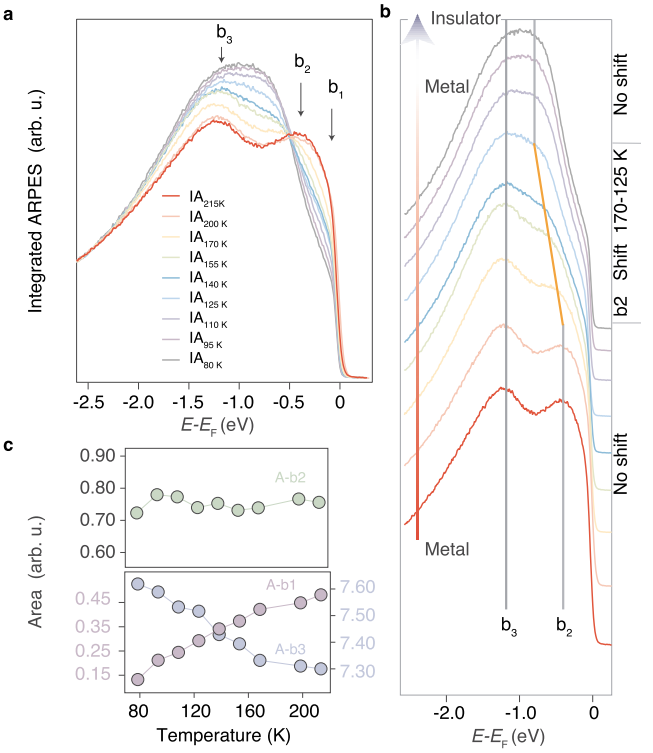

Figure 4. (a) Angle-integrated photoemission intensity as a function of temperature showing the evolution of the bands detected as a function of temperature. (b) Waterfall plot of the integrated intensity showing the energy shift of the band b_2 as a function on temperature. (c) Spectral intensity of b_1, b_2, and b_3 as a function of temperature.

With decreasing temperature, b_1, b_2, and b_3 bands evolve differently while temperature dependent GIXRD measurements show no evidence of the rhombohedral−monoclinic structural transformation reported in bulk and thicker films. Angle-integrated photoemission intensity of the b_i-bands shows a loss of spectral weight of the band b_1 and its transfer to the b_3 lower state (panels a−c in Figure 4). The b_3 band remains constant in energy, and negligible changes are observed in its dispersion, as also highlighted by the constant high-energy tail (Figure 3a,b). On the contrary, for b_2 we observe a large downward energy shift. Such a shift occurs between 170 and 125 K and stabilizes below 125 K. It is possible that this energy shift can still develop further, but we do not observe this within our energy and momentum resolutions (~15 meV and 0.02 $Å^{-1}$, respectively) and the evident broadening of our data. This behavior is suggestive of an effective increase of the trigonal crystal field splitting that pushes down in energy the e_g^{π} orbital, in agreement with the LDA-DMFT prediction,[16] although we cannot see a corresponding upward shift of the a_g^1, which is prevented by the dead layer mechanism. What we find remarkable is that such purported enhancement of the trigonal field is not gradual but occurs in a rather narrow temperature range. Even more remarkable is the lack of evidence of a downward shift of the quasiparticle b_1 band at the Fermi level, which we find has also e_g^{π} character. This suggests that the transition from the high temperature metal to the low temperature Mott insulator that we observe is not entirely similar to the one predicted from the paramagnetic metal to the paramagnetic insulator upon rising the Hubbard U.[16] In other words, although the energy shift of the b_2 band is compatible with an enhancement of trigonal

https://doi.org/10.1021/acs.nanolett.2c02288
Nano Lett. 2022, 22, 5990−5996

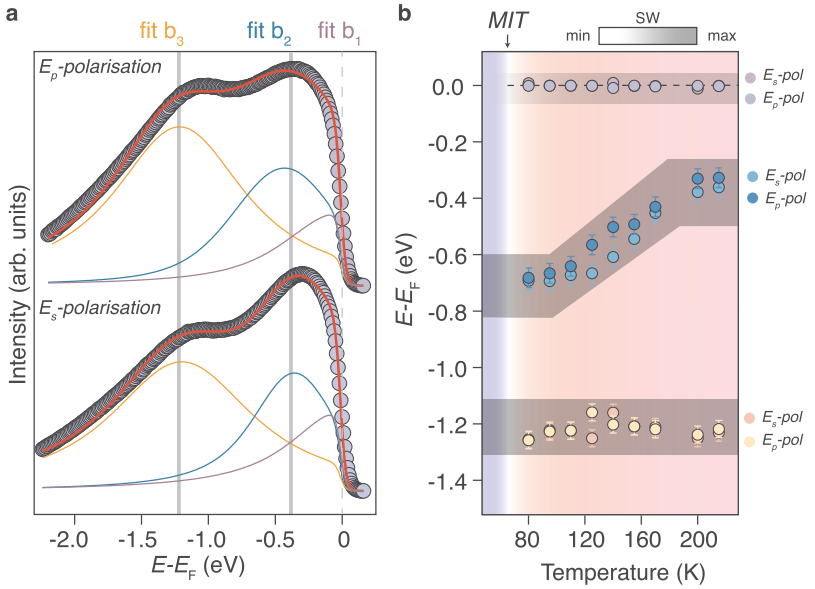

Figure 5. (a) Details of the fits executed for the *k*-integrated ARPES intensity, for both E_s and E_p polarized light. The minimum model includes three broad peaks. Each peak is described by a Voigt shape (Lorentzian convoluted by a Gaussian to account for the instrumental resolutions). A Fermi edge has been taken into account. (b) Energy positions of the centroid of the bands b_1, b_2, and b_3.

field, such an enhancement seems ineffective at low energy, at least for the e_g^{π} orbital, possibly because it is compensated by the diminishing quasiparticle residue.

This behavior is summarized in Figure 5, where after fitting the *k*-integrated ARPES intensity, i.e., mimicking the density of states (DOS), with a minimal set of three Lorentzian components (Figure 5a) in Figure 5b, we include the results of the peak energy positions as a function of temperature for both E_s and E_p light polarizations (the same fitting procedure was also used to obtain the data in Figure 4c).

Should the center of gravity of b_2 follow the same linear decrease of b_1 spectral weight, one could possibly attribute such behavior to coexisting insulator and metal domains, the fraction of the latter linearly vanishing at the transition. However, the substantial energy shift of b_2 that occurs in a narrow temperature window relative to the slow linear decrease of b_1 spectral weight rules out that scenario.[20,32] Moreover, from fitting results, there is no evidence of a double-peak structure underneath b_2 to suggest a spectral weight transferring between two energy-locked bands as a function of temperature, therefore ruling out a direct correlation with that related to b_1–b_3 bands. In addition, the coexistence of two different electronic environments being present would be directly detected by ARPES.[33] Our observation is therefore reminiscent of a genuine Mott-like transition[34,34,35] that occurs when the band b_1 that is crossing the Fermi level loses all its spectral weight. We emphasize that such a conclusion has the caveat that, as earlier mentioned, we cannot access the evolution at the Fermi level of the a_g^1 orbital. Importantly, we also found analogous results for samples of similar thickness but grown in a different partial O_2 pressure with the only effect to move up (when grown at lower O_2 pressure) and down (when grown at higher O_2 pressure) the critical temperature at which the b_1-to-b_3 transfer of spectral weight occurs.[27,36]

In conclusion, by exploiting in situ high-precision growth, we were able to freeze our V_2O_3 this films in the corundum phase and thus avoid the structural transformation occurring in the bulk system. This in turn allowed us to observe the purely electronic dynamics across the metal–insulator transition that resembles the textbook example of a nonsymmetry breaking Mott transition as revealed by DMFT.[21] Indeed, the particular low-temperature magnetic order in bulk V_2O_3 is believed to be a consequence of a substantial magnetic frustration that is resolved only by the C3 symmetry breaking at the rhombohedral–monoclinic transition.[36−38] We cannot exclude that once the structural transformation is circumvented (as in our thin film regime), the magnetic transition is pushed below the metal–insulator one, which would render the observed MIT a genuine paramagnetic Mott transition. Understanding and controlling such an electronic transition are fundamental to enable novel emergent phases of matter, with the confluence of magnetism, correlations, and magnetic frustration.

■ ASSOCIATED CONTENT

Supporting Information

The Supporting Information is available free of charge at https://pubs.acs.org/doi/10.1021/acs.nanolett.2c02288.

Characterization of the samples, temperature dependent GIXRD measurements, resistivity as a function of thickness and oxygen content, ARPES spectra with E_d polarization, an overview of the ARPES bands that form the electronic structure of V_2O_3, ARPES measureents at different photon energies, ARPES Fermi surfaces, XRD data and thickness dependence, and quasi-particle residue analysis (PDF)

■ AUTHOR INFORMATION

Corresponding Author

Federico Mazzola − *CNR-IOM, I-34149 Trieste, Italy;* orcid.org/0000-0002-5380-4374; Email: mazzola@iom.cnr.it

Authors

Sandeep Kumar Chaluvadi − *CNR-IOM, I-34149 Trieste, Italy;* orcid.org/0000-0002-3689-3336

Vincent Polewczyk − *CNR-IOM, I-34149 Trieste, Italy*

https://doi.org/10.1021/acs.nanolett.2c02288
Nano Lett. 2022, 22, 5990−5996

Debashis Mondal − *CNR-IOM, I-34149 Trieste, Italy*
Jun Fujii − *CNR-IOM, I-34149 Trieste, Italy*
Piu Rajak − *CNR-IOM, I-34149 Trieste, Italy*
Mahabul Islam − *CNR-IOM, I-34149 Trieste, Italy*
Regina Ciancio − *CNR-IOM, I-34149 Trieste, Italy;* orcid.org/0000-0003-1739-3763
Luisa Barba − *Istituto di Cristallografia del CNR, I-34149 Trieste, Italy*
Michele Fabrizio − *International School for Advanced Studies (SISSA), I-34149 Trieste, Italy*
Giorgio Rossi − *University of Milano, I-20133 Milano, Italy; CNR-IOM, I-34149 Trieste, Italy;* orcid.org/0000-0002-9330-7436
Pasquale Orgiani − *CNR-IOM, I-34149 Trieste, Italy;* orcid.org/0000-0002-1082-9651
Ivana Vobornik − *CNR-IOM, I-34149 Trieste, Italy*

Complete contact information is available at: https://pubs.acs.org/10.1021/acs.nanolett.2c02288

Author Contributions

[⊥]F.M. and S.K.C. contributed equally to this work. F.M., S.K.C., and D.M. performed ARPES experiments and analyzed the ARPES data, with contributions and guidance by G.R., J.F., and I.V.; F.M., S.K.C., and P.O. grew the samples by PLD; L.B. and P.O. measured XRD. P.R., M.I., and R.C. measured and analyzed the TEM data; V.P. performed resistivity measurements. M.F. contributed to theoretical understanding. F.M., M.F., P.O., G.R., J.F., and I.V. wrote the manuscript with contributions from all the authors.

Notes

The authors declare no competing financial interest.

Data Availability. Authors confirm that all relevant data are included in the paper and/or its Supporting Information file.

■ ACKNOWLEDGMENTS

F.M. acknowledges Prof. Sergio di Matteo and Dr. Giancarlo Panaccione for useful discussions on the topics. Ezio Cociancich, Federico Salvador, and Giuseppe Chita are acknowledged for technical support. This work has been performed in the framework of the nanoscience foundry and fine-analysis (NFFA-MIUR Italy Progetti Internazionali) facility. M.F. has received funding from the European Research Council (ERC) under the European Union's Horizon 2020 Research and Innovation Programme, Grant Agreement 692670 "FIRSTORM".

■ REFERENCES

(1) Dernier, P. D.; Marezio, M. Crystal structure of the low-temperature antiferromagnetic phase of V_2O_3. *Phys. Rev. B* **1970**, *2*, 3771−3776.
(2) Leonov, I.; Anisimov, V. I.; Vollhardt, D. Metal-insulator transition and lattice instability of paramagnetic V_2O_3. *Phys. Rev. B* **2015**, *91*, 195115.
(3) McWhan, D. B.; Rice, T. M.; Remeika, J. P. Mott Transition in Cr-Doped V_2O_3. *Phys. Rev. Lett.* **1969**, *23*, 1384−1387.
(4) McWhan, D. B.; Menth, A.; Remeika, J. P.; Brinkman, W. F.; Rice, T. M. Metal-Insulator Transitions in Pure and Doped V_2O_3. *Phys. Rev. B* **1973**, *7*, 1920−1931.
(5) Paolasini, L.; Vettier, C.; de Bergevin, F.; Yakhou, F.; Mannix, D.; Stunault, A.; Neubeck, W.; Altarelli, M.; Fabrizio, M.; Metcalf, P. A.; Honig, J. M. Orbital Occupancy Order in V_2O_3: Resonant X-Ray Scattering Results. *Phys. Rev. Lett.* **1999**, *82*, 4719−4722.
(6) Meneghini, C.; Di Matteo, S.; Monesi, C.; Neisius, T.; Paolasini, L.; Mobilio, S.; Natoli, C. R.; Metcalf, P. A.; Honig, J. M. Structural dichroism in the antiferromagnetic insulating phase of V_2O_3. *Phys. Rev. B* **2005**, *72*, 033111.
(7) Yuan, J.; Hu, X.; Li, J.; Liu, Y.; Zhong, G.; Huang, T. V_2O_3 nanoparticles confined in high-conductivity and high-throughput carbon nanofiber nanohybrids for advanced sodium-ion capacitors. *ACS Appl. Mater. Interfaces* **2021**, *13*, 10001−10012.
(8) Lee, M. H.; Kalcheim, Y.; Valle, J. D.; Schuller, I. K. Controlling metal-insulator transitions in vanadium oxide thin films by modifying oxygen stoichiometry. *ACS Appl. Mater. Interfaces* **2021**, *13*, 887−896.
(9) Ronchi, A.; Homm, P.; Menghini, M.; Franceschini, P.; Maccherozzi, F.; Banfi, F.; Ferrini, G.; Cilento, F.; Parmigiani, F.; Dhesi, S. S.; Fabrizio, M.; Locquet, J.-P.; Giannetti, C. Early-stage dynamics of metallic droplets embedded in the nanotextured Mott in V_2O_3. *Phys. Rev. B* **2019**, *100*, 075111.
(10) Zhou, Y.; Ramanathan, S. Mott Memory and Neuromorphic Devices. *Proc. IEEE* **2015**, *103*, 1289−1310.
(11) Luo, H.; Wang, B.; Wang, F.; Yang, J.; Wu, F.; Ning, Y.; Zhou, Y.; Wang, D.; Liu, H.; Dou, S. Anodic Oxidation Strategy toward Structure-Optimized V_2O_3 Cathode via Electrolyte Regulation for Zn-Ion Storage. *ACS Nano* **2020**, *14*, 7328−7337.
(12) Rice, C. E.; Robinson, W. R. Structural changes in the solid solution $(Ti_{1-x}V_x)_2O_3$ as x varies from zero to one. *J. Solid State Chem.* **1977**, *21*, 145−154.
(13) Robinson, W. R. High-temperature crystal chemistry of V_2O_3 and 1% chromium-doped V_2O_3. *Acta Crystallogr. B* **1975**, *31*, 1153−1160.
(14) Mott, N. F. Metal-Insulator Transition. *Rev. Mod. Phys.* **1968**, *40*, 677−683.
(15) Dillemans, L.; Smets, T.; Lieten, R. R.; Menghini, M.; Su, C.-Y.; Locquet, J.-P. Evidence of the metal-insulator transition in ultrathin unstrained V_2O_3 thin films. *Appl. Phys. Lett.* **2014**, *104*, 071902.
(16) Poteryaev, A. I.; Tomczak, J. M.; Biermann, S.; Georges, A.; Lichtenstein, A. I.; Rubtsov, A. N.; Saha-Dasgupta, T.; Andersen, O. K. Enhanced crystal-field splitting and orbital-selective coherence induced by strong correlations in V_2O_3. *Phys. Rev. B* **2007**, *76*, 085127.
(17) Lantz, G.; et al. Ultrafast evolution and transient phases of a prototype out-of-equilibrium Mott−Hubbard material. *Nat. Commun.* **2017**, *8*, 13917.
(18) Lo Vecchio, I.; Denlinger, J. D.; Krupin, O.; Kim, B. J.; Metcalf, P. A.; Lupi, S.; Allen, J. W.; Lanzara, A. Fermi Surface of Metallic V_2O_3 from Angle-Resolved Photoemission: Mid-level Filling of e_g^{π} Bands. *Phys. Rev. Lett.* **2016**, *117*, 166401.
(19) Majid, S. S.; Shukla, D. K.; Rahman, F.; Gautam, K.; Choudhary, R. J.; Sathe, V. G.; Phase, D. M. Stabilization of metallic phase in V_2O_3 thin film. *Appl. Phys. Lett.* **2017**, *110*, 173101.
(20) McLeod, A. S.; van Heumen, E.; Ramirez, J. G.; Wang, S.; Saerbeck, T.; Guenon, S.; Goldflam, M.; Anderegg, L.; Kelly, P.; Mueller, A.; Liu, M. K.; Schuller, I. K.; Basov, D. N. Nanotextured phase coexistence in the correlated insulator V_2O_3. *Nat. Phys.* **2017**, *13*, 80−86.
(21) Georges, A.; Kotliar, G.; Krauth, W.; Rozenberg, M. J. Dynamical mean-field theory of strongly correlated fermion systems and the limit of infinite dimensions. *Rev. Mod. Phys.* **1996**, *68*, 13−125.
(22) Chaluvadi, S. K.; Mondal, D.; Bigi, C.; Knez, D.; Rajak, P.; Ciancio, R.; Fujii, J.; Panaccione, G.; Vobornik, I.; Rossi, G.; Orgiani, P. Pulsed laser deposition of oxide and metallic thin films by means of Nd:YAG laser source operating at its 1st harmonics: recent approaches and advances. *J. Phys.: Mater.* **2021**, *4*, 032001.
(23) Caputo, M.; Jandke, J.; Cappelli, E.; Chaluvadi, S.; Bonini Guedes, E.; Naamneh, M.; Vinai, G.; Fujii, J.; Torelli, P.; Vobornik, I.; Goldoni, A.; Orgiani, P.; Baumberger, F.; Radovic, M.; Panaccione, G. Metal to insulator transition at the surface of V_2O_3 thin films: An in-situ view. *Appl. Surf. Sci.* **2022**, *574*, 151608.
(24) Giorgianni, F.; Udina, M.; Cea, T.; Paris, E.; Caputo, M.; Radovic, M.; Boie, L.; Sakai, J.; Schneider, C. W.; Johnson, S. L. Terahertz displacive excitation of a coherent Raman-active phonon in V_2O_3. *Commun. Phys.* **2022**, *5*, 103.

(25) Rozier, P.; Ratuszna, A.; Galy, J. Comparative Structural and Electrical Studies of V_2O_2 and $V_{2-x}Ni_xO_3$ (0< x <0.75) Solid SolutionDedicated to Professor Joachim Strähle on the Occasion of his 65th Birthday. *Zeitschrift für anorganische und allgemeine Chemie* **2002**, *628*, 1236.
(26) Finger, L. W.; Hazen, R. M. Crystal structure and compression of ruby to 46 kbar. *J. Appl. Phys.* **1978**, *49*, 5823−5826.
(27) Thorsteinsson, E. B.; Shayestehaminzadeh, S.; Arnalds, U. B. Tuning metal-insulator transitions in epitaxial V_2O_3 thin films. *Appl. Phys. Lett.* **2018**, *112*, 161902.
(28) Kimizuka, N.; Ishii, M.; Saeki, M.; Nakano, M.; Nakahira, M. The metal/antiferromagnetic insulator transition of V2O3 as affected by the non-stoichiometry and Ti-, Cr- and Fe-doping. *Solid State Commun.* **1973**, *12*, 43−46.
(29) Park, J.-H.; Tjeng, L. H.; Tanaka, A.; Allen, J. W.; Chen, C. T.; Metcalf, P.; Honig, J. M.; de Groot, F. M. F.; Sawatzky, G. A. Spin and orbital occupation and phase transitions in V_2O_3. *Phys. Rev. B* **2000**, *61*, 11506−11509.
(30) Borghi, G.; Fabrizio, M.; Tosatti, E. Surface dead layer for quasiparticles near a Mott transition. *Phys. Rev. Lett.* **2009**, *102*, 066806.
(31) Rodolakis, F.; Mansart, B.; Papalazarou, E.; Gorovikov, S.; Vilmercati, P.; Petaccia, L.; Goldoni, A.; Rueff, J. P.; Lupi, S.; Metcalf, P.; Marsi, M. Quasiparticles at the Mott Transition in V_2O_3: Wave Vector Dependence and Surface Attenuation. *Phys. Rev. Lett.* **2009**, *102*, 066805.
(32) Thees, M.; et al. Imaging the itinerant-to-localized transmutation of electrons across the metal-to-insulator transition in V_2O_3. *Sci. Adv.* **2021**, *7*, 1−8.
(33) Mazzola, F.; Sunko, V.; Khim, S.; Rosner, H.; Kushwaha, P.; Clark, O. J.; Bawden, L.; Marković, I.; Kim, T. K.; Hoesch, M.; Mackenzie, A. P.; King, P. D. C. Itinerant ferromagnetism of the Pd-terminated polar surface of PdCoO 2. *Proc. Natl. Acad. Sci. U. S. A.* **2018**, *115*, 12956−12960.
(34) Meyer, R.; Zurhelle, A. F.; De Souza, R. A.; Waser, R.; Gunkel, F. Dynamics of the metal-insulator transition of donor-doped $SrTiO_3$. *Phys. Rev. B* **2016**, *94*, 115408.
(35) Brouet, V.; Mansart, J.; Perfetti, L.; Piovera, C.; Vobornik, I.; Le Fèvre, P.; Bertran, F.; Riggs, S. C.; Shapiro, M. C.; Giraldo-Gallo, P.; Fisher, I. R. Transfer of spectral weight across the gap of Sr_2IrO_4 induced by La doping. *Phys. Rev. B* **2015**, *92*, 081117.
(36) Leiner, J. C.; Jeschke, H. O.; Valentí, R.; Zhang, S.; Savici, A. T.; Lin, J. Y. Y.; Stone, M. B.; Lumsden, M. D.; Hong, J.; Delaire, O.; Bao, W.; Broholm, C. L. Frustrated Magnetism in Mott Insulating $(V_{1-x}Cr_x)_2O_3$. *Physical Review X* **2019**, *9*, 011035.
(37) Grieger, D.; Piefke, C.; Peil, O. E.; Lechermann, F. Approaching finite-temperature phase diagrams of strongly correlated materials: A case study for V_2O_3. *Phys. Rev. B* **2012**, *86*, 155121.
(38) Grieger, D.; Fabrizio, M. Low-temperature magnetic ordering and structural distortions in vanadium sesquioxide V_2O_3. *Phys. Rev. B* **2015**, *92*, 075121.

https://doi.org/10.1021/acs.nanolett.2c02288
Nano Lett. 2022, 22, 5990−5996